Selective Laser Melting Microstructure Sensitivity Analysis to Process Parameters of Hastelloy X using Cellular Automata

Burim Dervishaj

Semester Project
08.11.2021

Dr. Ehsan Hosseini
Jian Tang

Prof. Dr. Edoardo Mazza

Abstract

Additive Manufacturing methods like Selective Laser Melting are modern and continuously growing manufacturing techniques specialized in the production of highly complex components. With its layer-by-layer approach Selective Laser Melting is very well suited for prototyping as well as production of intricate geometries. Due to the high temperature gradients and fast cooling rates the parts are expected to have very fine microstructure. The parts are also assumed to have a high degree of anisotropy caused by the systematic temperature gradients present during solidification. To predict the response of SLM manufactured parts, simulations have been developed. In this project one such simulation based on the algorithm of Cellular Automata for SLM single tracks was used for microstructure prediction. The generated microstructure data was then analyzed using the Principal Component Analysis (PCA) and validated with experimental data. This analysis was split into two main parts, namely the three- and the two-dimensional analysis. For the three-dimensional analysis the grain shape was quantified using PCA. The two-dimensional quantification determined the grain shape as well as the crystallographic grain orientation using Texture plots. Afterwards, a sensitivity analysis of Microstructure to Process Parameters was conducted, and the two-dimensional results were compared with experimental data.

ETH

Eidgenössische Technische Hochschule Zürich
Swiss Federal Institute of Technology Zurich

Declaration of originality

The signed declaration of originality is a component of every semester paper, Bachelor's thesis, Master's thesis and any other degree paper undertaken during the course of studies, including the respective electronic versions.

Lecturers may also require a declaration of originality for other written papers compiled for their courses.

I hereby confirm that I am the sole author of the written work here enclosed and that I have compiled it in my own words. Parts excepted are corrections of form and content by the supervisor.

Title of work (in block letters):

Selective Laser Melting Microstructure Sensitivity Analysis to Process Parameters of Hastelloy X using Cellular Automata

Authored by (in block letters):
For papers written by groups the names of all authors are required.

Name(s):	**First name(s):**
Dervishaj	Burim

With my signature I confirm that
   - I have committed none of the forms of plagiarism described in the 'Citation etiquette' information sheet.
   - I have documented all methods, data and processes truthfully.
   - I have not manipulated any data.
   - I have mentioned all persons who were significant facilitators of the work.

I am aware that the work may be screened electronically for plagiarism.

Place, date	**Signature(s)**
08.11.2021	*Bu.Dervishaj*

For papers written by groups the names of all authors are required. Their signatures collectively guarantee the entire content of the written paper.

Contents

List of Figures

List of Tables

1

Motivation

Additive Manufacturing techniques like Selective Laser Melting have proven to be able to produce very complex parts, opening a new dimension in the design space of part manufacturing. The SLM-process employs a layer-by-layer strategy where a part is created one layer at a time.

The process starts by applying a powder layer to the substrate plate. A laser source then melts the selective areas of the powder layer. The molten areas then combine with the underlying material to form the part. This is also where the name "Additive Manufacturing" comes from since material is only added to the part and never removed. This is a big contrast to conventional manufacturing techniques where the process usually starts with a block of raw material, that is then worked into shape by removing material. This leads to higher waste since most of the removed material can't be reused immediately. Because of these benefits Selective Laser Melting finds good use in prototyping. Due to its slow building rates SLM is not suited for large batch size production.

The layer-by-layer approach also causes the production rate of Selective Laser Melting to not be dependent on complexity of the geometry. The downside to this are slow building rates for very simple dense parts. Adding to that, another drawback are the high acquisition and material costs which make it difficult for new companies to incorporate Selective Laser Melting into their manufacturing process. Therefore, a deep understanding and an optimal virtual depiction of the entire process using simulations is of high importance. This would allow companies to decide in advance whether they want to use Additive Manufacturing and in general make it more attractive as a manufacturing alternative.

2

In this Semester Project an existing single track microstructure simulation for Selective Laser Melting based on Cellular Automata was used for a sensitivity analysis of microstructure to process parameters. To this end, a fully automated tool was created in MATLAB that incorporates thermal simulations from Abaqus with microstructure simulations in MATLAB. Subsequently, the generated simulation data was evaluated with a principal component analysis to get a representative quantification of the three-dimensional grain structure. Afterwards, a texture analysis of multiple sections in the laser track was conducted using the MATLAB toolbox MTEX. Lastly, experimental data was also analyzed using the principal component analysis and then compared to the simulation results.

2

Theoretical Foundation

In this chapter an overview of the properties of Hastelloy X will be given. Afterwards, the general Selective Laser Melting process will be explained in detail. Lastly, the algorithm used for the generation of the microstructure prediction will be described.

2.1 Hastelloy X

Hastelloy X is a solid solution strengthened Nickel based superalloy. It is a commonly used material in gas turbine engines as well as in the chemical process industry. This is mostly due to its high oxidation resistance and high strength at elevated temperatures [3]. Hastelloy X was used because it can withstand the high temperature gradients and fast cooling rates of the Selective Laser Melting process. After solidification a strongly columnar dendritic microstructure is observed. This causes Hastelloy X parts produced with Selective Laser Melting to have higher yield strength and hardness than its conventionally manufactured counterparts [4,5]. A downside is the material's susceptibility to cracks in high temperature manufacturing, also known as hot-cracking. This can be partially overcome by employing a post processing technique called hot isostatic pressing (HIP) where the part is pressed together with high pressure at an elevated temperature to close pores and cracks [3].

2.2 Selective Laser Melting

2.2.1 General procedure

Selective Laser Melting is a powder based additive manufacturing technique. A schematic representation of the process can be found in **Figure 2.1**.

First, a 3D-CAD model of the part to be manufactured is created. Afterwards, that model is sliced into equally sized layers using a Slicing program. These slices act as the main building blocks, in which specific areas are later molten into a connected part. With this the first layer is ready to be applied onto the build platform. To this end the metal powder supply platform is raised and the build platform is lowered by the desired layer thickness. Then the recoater arm sweeps over the build platform covering it in a powder layer with the desired layer thickness. Any excess powder is swept into a container and stored for later use. With the layer applied the laser source starts to melt the selective areas that were predefined by the sliced 3D-CAD model. The laser's position is controlled by a scanning mirror that can be rotated to ensure proper positioning. After the laser has molten all areas in this layer the process is paused to give the material enough time to cool down. When everything has sufficiently cooled down the cycle starts anew by raising the metal powder supply and lowering the build platform by another layer thickness. This is repeated until the part is finished. The not yet molten powder is then sifted and stored in a powder container. [1]
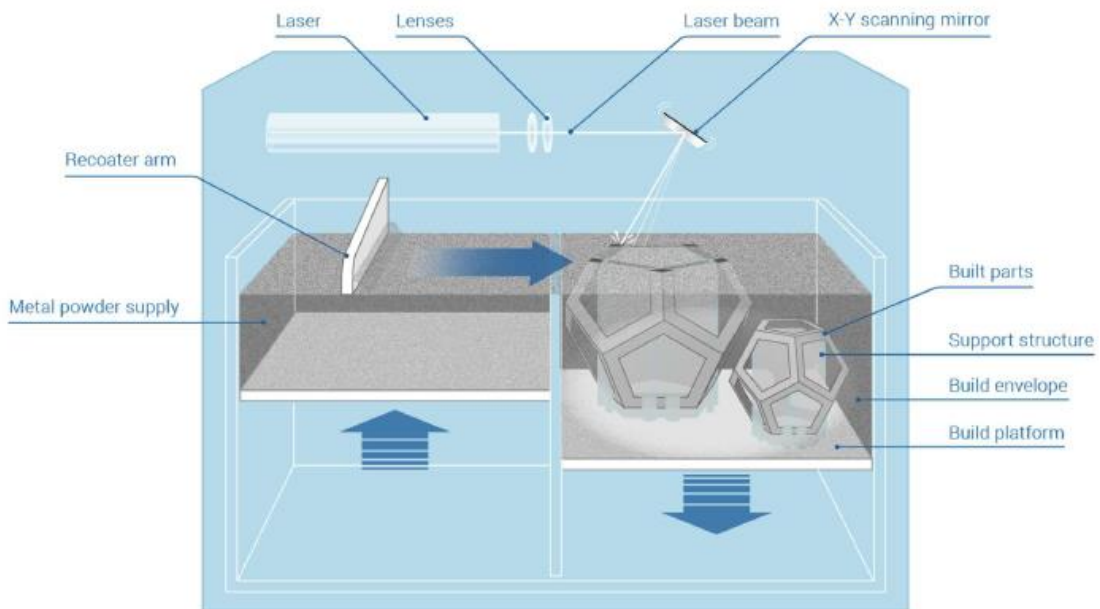
Figure 2.1: Schematic representation of the general Selective Laser Melting process [2]

2.2.2 Mechanical properties

The mechanical properties of Selective Laser Melting manufactured parts are highly dependent on the chosen process parameters. They are also expected to be very anisotropic due to the columnar microstructure and strong texture that is formed during SLM solidification. The high temperature gradients and rapid cooling rates can cause materials to start cracking during solidification. A high energy density leads to the presence of key-hole pores [3]. The cracks and pores are two effects that negatively impact the mechanical properties of SLM manufactured parts. As mentioned in the material section defects, like cracks and Lack of Fusions defects, can be partially circumvented using post processing techniques like hot isostatic pressing [3].

2.3 Microstructure simulation

There are two main types of numerical methods used for simulation of complex dendritic solidification processes, namely the stochastic and the deterministic methods. A commonly used deterministic method is the phase field modeling method, in which a field variable smoothly varies over the interface between different phases [8]. This method has been used to model the growth of dendrite structures in pure materials and alloys [10]. The downside to deterministic methods like the phase field method are their high computational costs. Because of the high computational effort needed, these approaches are usually restricted to small length scale and small number of grains [8]. To overcome these issues stochastic methods, offer a good alternative. Due to the nature of stochastic methods their computational effort required is in general lower than the required effort of deterministic methods. Which is why the microstructure prediction of Selective Laser Melting produced parts is commonly based on stochastic methods [8]. One of the most popular stochastic methods is the Cellular Automata (CA) algorithm, which will be explained in detail in the following chapter.

In this project an existing Selective Laser Melting single track microstructure simulation created by J. Tang was used. This simulation is based on the principles of Cellular Automata. A schematic representation of the general microstructure simulation Process can be found in **Figure 2.2**.
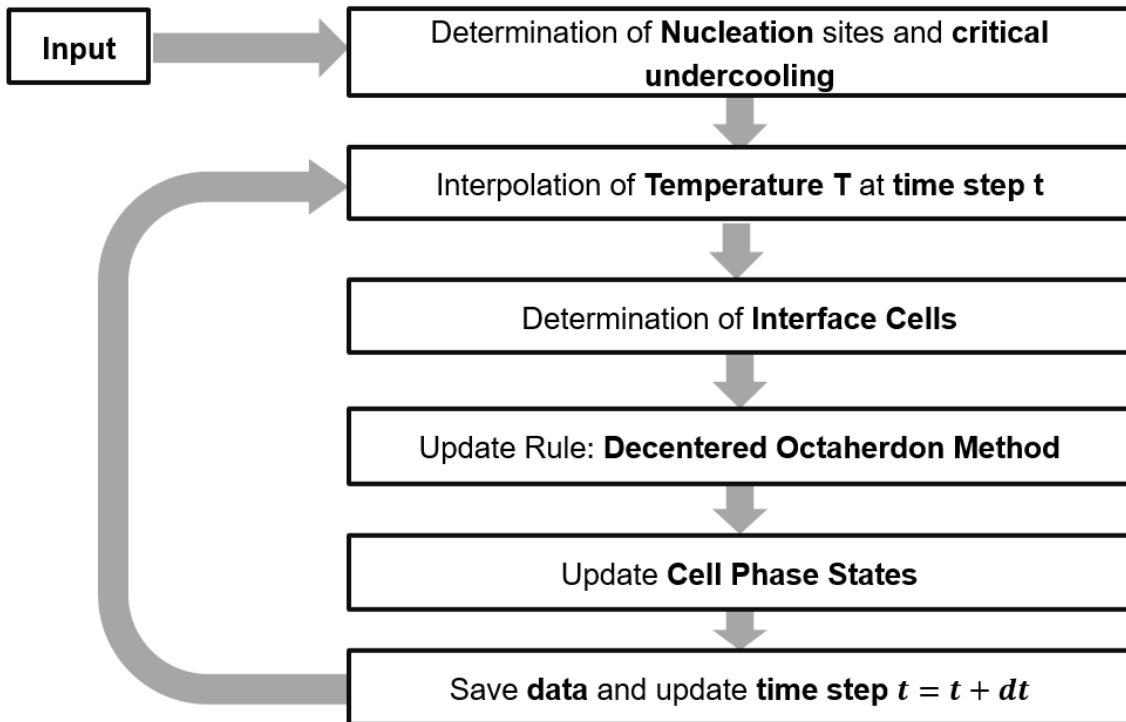
Figure 2.2: Schematic representation of the general Cellular Automata algorithm

2.3.1 Cellular Automata (CA)

Cellular Automata are dynamic systems in which time, space and states are discrete [13].

First, the simulation space is subdivided into equally sized cells. A finite number of states can then be assigned to each cell. The states that were used in the simulation are: phase, undercooling, center point of the Update Rule and crystallographic orientation. These states cannot be changed during a time step. One of the most important aspects of Cellular Automata is its locality since each cell can only interact with a predefined number of neighboring cells [13]. This link between the neighboring cells is called the Update Rule.

2.3.2 Update Rule

To calculate the states of a cell at a given time step, Update Rules were developed, which provide a link between the states of the current cell and the states of the neighboring cells. The neighboring cells of a center cell are determined based on so called Neighborhood Rules. In this sub-chapter one

Update Rule and two Neighborhood Rules will be presented: the Moore Neighborhood Rule, the Von-Neumann Neighborhood Rule and the decentered octahedron Update Rule.

The Moore and Von-Neumann Neighborhood Rules are in general very similar. The Von-Neumann Neighborhood Rule defines that only the six closest cells have an influence on the center cell. This Neighborhood Rule can also be used as an Update Rule. In the words of Selective Laser Melting, if the center cell changes its phase state from 0 (Interface) to 1 (Solid) then the predefined neighbor cells that are not fully solidified or not already in the interface change their phase state to interface. The Moore Neighborhood Rule follows a similar pattern. In the Moore Neighborhood Rule the only difference is that all neighboring cells have influence on the states of the center cell. So, for the Moore Neighborhood Rule all 26 surrounding cells count as neighbor cells. If these two Neighborhood Rules are used as Update Rules, they form a very basic Cellular Automata algorithm. These Update Rules are not very well suited for simulation of solidification processes in Selective Laser Melting since they can't capture the influence of many physical properties like the preferred growth direction of a grain during solidification or its crystallographic orientation. Therefore, these Update Rules were not implemented in the Cellular Automata algorithm that was used in this project. A two-dimensional schematic representation of the Moore and Von-Neumann neighborhood Update Rules can be found in **Figure 2.3**.
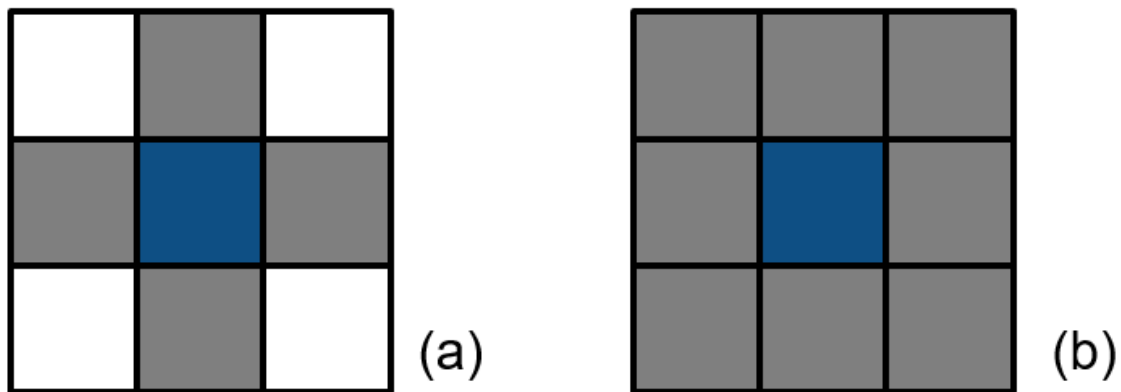
Figure 2.3: Two-dimensional schematic representation of the Update Rules: (a) Von-Neumann and (b) Moore neighborhood for cubic cells

In decentered octahedron Update Rule a virtual octahedron is created at the center of each nucleating cell. This octahedron will have the same orientation as the grain's crystallographic orientation. It grows with increasing solidification of the cell. Once the cell is fully solidified the octahedron stops growing and the cell state is set to Solid. If this virtual octahedron captures a neighboring liquid cell's center point it will instantiate a new octahedron centered on the connection line between the two center points. This approach is very well suited for microstructure simulation during solidification since the octahedron can imitate physical properties like the aforementioned preferred growth direction of grains

and their crystallographic orientation. A schematic depiction of this method can be found in **Figure 2.4.**
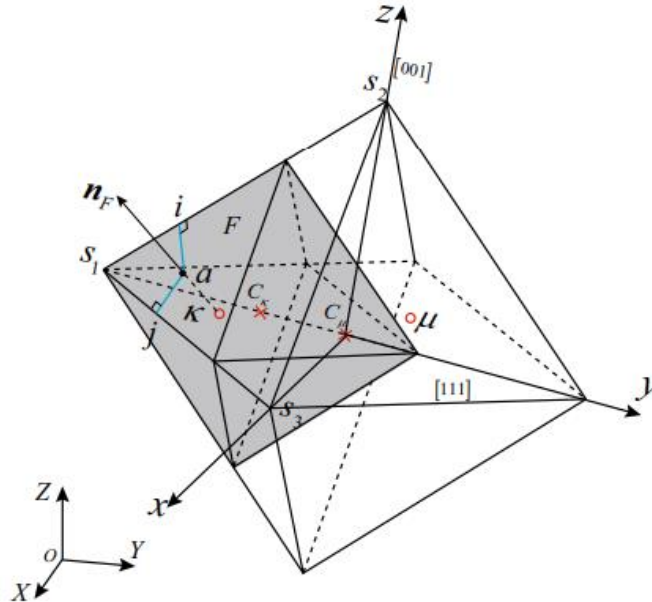
Figure 2.4: Schematic representation of the decenetered octahedron Upate Rule [8].

2.3.3 Nucleation and Grain Growth

Implementation of nucleation and grain growth is based on [8].

In Cellular Automata, nucleation needs to be predefined for the algorithm to work. To this end, in the initialization of the simulation potential nucleation sites are chosen. These sites are randomly picked from all possible cells with the amount of potential nucleation sites calculated as:

$$N_v = \varrho_v * V$$

(2.1)

Where ϱ_v is the nucleation density for bulk and V represent the total bulk liquid volume. Each of these potential nucleation sites is then assigned a critical undercooling, which follows a gaussian distribution with mean value and standard deviation (ΔT_{max} and ΔT_σ). This critical undercooling gives the cell a value at which it will start nucleating to form a grain. If a cell is chosen multiple times as a nucleation site, then the smallest selected critical undercooling will be chosen instead [8].

Nucleation takes place once a nucleation cell has reached an undercooling that is greater or equal to its critical undercooling. Afterwards this cell is assigned a randomly picked crystallographic orientation and a virtual octahedron of size 0 is generated at the center point. That octahedron is then oriented to match the crystallographic orientation of the cell.

Once the nucleation cells have been activated grain growth starts by setting their phase state variable to 0 (Interface). Grain growth is governed by the dendrite tip growth kinetics [8] so a definition for dendrite growth velocity needs to be determined. As proposed by [16] the dendrite growth velocity v was calculated as follows:

$$v(\Delta T) = \eta_2 * \Delta T^2 + \eta_3 * \Delta T^3 \tag{2.2}$$

Where η_2 and η_3 are coefficients with units $\frac{m}{s*K^2}$ and $\frac{m}{s*K^3}$ and ΔT is the current undercooling.

During grain growth the decentered octahedron Update Rule is performed in every timestep and on every interface cell. The size of the octahedron L_v is calculated as:

$$L_v(t) = \frac{1}{\sqrt{3}} \int_{t_v}^{t} v\big(\Delta T(\tau)\big) d\tau \tag{2.3}$$

Where v is the dendrite growth velocity calculated using **Equation (2.2)**, t is the current time step and t_v is the time at which this cell started to solidify. Once a liquid cell's center point is enveloped by an octahedron it will start to solidify as well, changing its phase state to 0 (Interface) and creating its own octahedron with the inherited crystallographic orientation of the capturing cell. These two cells will be considered as belonging to the same grain.

Implementation of the decentered octahedron Update Rule follows the algorithm proposed by [17]. If we take the two cells μ and κ shown in **Figure 2.4**. with center points C_μ and C_κ, respectively.

The envelop size of cell μ at time step t is given as:

$$L_\mu(t) = L_\mu\big(t_\mu\big) + \frac{1}{\sqrt{3}} \int_{t_\mu}^{t} v\big(\Delta T(\tau)\big) * d\tau \tag{2.4}$$

Where $L_\mu(t_\mu)$ is the initial size of the envelope at cell μ, created at the time it was captured t_μ.

To initialize a captured cell κ the procedure (Update Rule) based on [8] and [17] is used:

1.)

Transformation of coordinate of cell center κ to local coordinate system associated with the envelop:

$$x^\kappa = M^T * (X^\kappa + X^{C_\mu})$$
(2.5)

Where X and x represent the coordinates of the cell center in global and local coordinate systems and M the orthogonal coordinate rotation matrix given by the Euler angles of μ.

2.) Determine in which octant C_κ is located and calculate the nearest octahedral face F to that center point.

3.) Calculate the distance between κ and the closest face with normal $\boldsymbol{n}_F$ as:

$$d = \frac{1}{\sqrt{3}}(hx_1^\kappa + kx_2^\kappa + lx_3^\kappa - \sqrt{3}L_\mu(t))$$
(2.6)

where $\sqrt{3}L_\mu(t)$ is the half-diagonal length of the envelope of cell μ and $[h, k, l]$ are the Miller indices of the closest octahedral face.

4.) Project the cell center of κ onto F denoted as the point a:

$$x^a = x^\kappa + \frac{1}{\sqrt{3}}|d|\boldsymbol{n}_F$$
(2.7)

5.) Ascertain the closest corner of the face s_1.

6.) Calculation of the projection of point a onto the edges $s_1 s_2$ and $s_1 s_3$. These projections will be denoted as I and J.

$$\overrightarrow{I_{s_1}} = \frac{(x^{s_2} - x^{s_1}) * (x^a - x^{s_1})}{\|(x^{s_2} - x^{s_1})\|^2}(x^{s_2} - x^{s_1})$$
(2.8)

$$\overrightarrow{J_{s_1}} = \frac{(x^{s_3} - x^{s_1}) * (x^a - x^{s_1})}{\|(x^{s_3} - x^{s_1})\|^2}(x^{s_3} - x^{s_1})$$
(2.9)

7.) New envelope size defined by two auxiliary variables:

$$L_{12} = \frac{1}{2}\left(Min\left[I_{s1}, \sqrt{3}d_{cell}\right] + Min\left[I_{s2}, \sqrt{3}d_{cell}\right]\right) \qquad (2.10)$$

$$L_{13} = \frac{1}{2}\left(Min\left[I_{s1}, \sqrt{3}d_{cell}\right] + Min\left[I_{s3}, \sqrt{3}d_{cell}\right]\right) \qquad (2.11)$$

The size of the new envelope edges is then calculated as:

$$L_{\kappa} = \sqrt{\frac{2}{3}}Max[L_{12}, L_{13}] \qquad (2.12)$$

8.) With the new octahedron size the center point of this octahedron can be computed as:

$$x^{C_{\kappa}} = \left(\lambda_{\mu} - \lambda_{\kappa}\right)\frac{\boldsymbol{n}_{OS1}}{\|\boldsymbol{n}_{OS1}\|} \qquad (2.13)$$

where $x^{C_{\kappa}}$ is the coordinate of the new grain octahedron and $\boldsymbol{n}_{0S1}$ represents the vector connecting o and s_1. The new center point's global coordinates can then be calculated as:

$$\boldsymbol{X}^{C_{\kappa}} = \boldsymbol{X}^{C_{\mu}} + \boldsymbol{M}\,\boldsymbol{x}^{C_{\kappa}} \qquad (2.14)$$

With this procedure a new envelope is created at κ.

3

Methods

In this chapter an overview of the methods used for the Sensitivity Analysis as well as for the microstructure quantification will be shown. First, the sampling strategies that were considered in this project will be explained. Afterwards, a detailed introduction to the methods used in the microstructure quantification will be given.

3.1 Design of Experiments (DOE)

To capture the whole complexity of the microstructure sensitivity to process parameters multiple Design of Experiments approaches were used. The DOEs considered in this project are the One-Factor-At-A-Time, the Full Factorial, and the Latin Hypercube sampling.

3.1.1 One-Factor-At-A-Time Design (OFAAT Design)

The One-Factor-At-A-Time sampling approach counts to the family of the systematic sampling approaches. Systematic approaches have a predefined sampling with no stochastic components. A schematic representation of a OFAAT sampling can be found in **Figure 3.1**.

OFAAT represents a very intuitive way to think about a problem. Contrary to most sampling strategies the OFAAT approach only varies one factor at a time. With this it is possible to conduct a sensitivity analysis of the system's dependence on a given parameter. If a system has multiple factors and is complex enough, then this strategy becomes obsolete, since it can only ever consider the effect of a single factor on the system at a time. Causing the design to be blind to the

interplay of different factors. Therefore, in most cases it is not efficient to use the OFAAT sampling techniques. As evident from **Figure 3.1**. finding an optimum with this sampling is very difficult. [18]
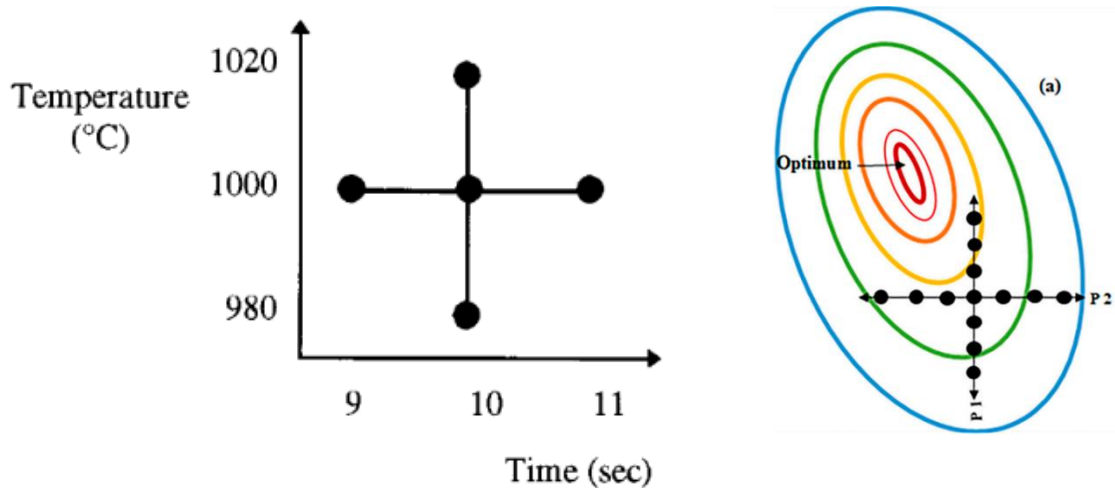
Figure 3.1: (left) One-Factor-At-A-Time with the design variables: Time and Temperature [18] (right) Schematic representation of optimization using One-Factor-At-A-Time approach [19]

Because of the high dependency on the initial guess as well as the lack of information of the interplay between different factors this approach was not further considered in this project.

3.1.2 Full Factorial Design (FF Design)

The Full Factorial Design also belongs to the family of systematic sampling strategies. It is very similar to the OFAAT approach. The main difference is that in the Full Factorial Design multiple factors are changed simultaneously.

To do a Full Factorial Design several values need to be defined for each parameter. These discrete values, also referred to as the levels of the factor, will be the only values the parameter can take. If, and only if, every factor has the same number of levels then the design is called symmetric factorial design [20] and the number of combinations is given as:

$$\#E = n^k \tag{3.1}$$

Here n are the levels of each factor and k are the number of factors. As evident from **Equation 3.1** the number of experiments scales exponentially with increasing k. Therefore, this sampling strategy is only efficient for small k. It is recommended to keep $k < 7$.

For an asymmetric factorial design, the general number of combinations is given by:

$$\#E = \prod_{i=1}^{k} n_i \qquad \textbf{(3.2)}$$

Here n_i represents the number of levels corresponding to factor i.

3.1.3 Latin Hypercube Design (LH Design)

Contrary to the already presented sampling techniques the Latin Hypercube Sampling count to the family of the stochastic sampling strategies. Therefore, the sampling achieved with LH is different every time. In the LH sampling all factors are varied at a time, making it possible to capture the entire complexity of the system.

Just like the FF design the LH sampling starts by defining the levels (n) of each factor. Importantly, all factors must have the same number of levels for the LH sampling to be applicable. Afterwards, a lower and upper bound is defined for each factor. The domain between the lower and upper bound is then subdivided into n equally sized intervals. The LH approach is then going to generate a sampling in which every interval of every factor is only going to be sampled once. The value of the factor inside an interval is randomly generated. A schematic representation of the Latin Hypercube sampling using two factors and ten intervals can be found in **Figure 3.2**.

As evident from the figure the sampling points are not allowed to share the same row or column. Since this is the only constraint on the generation of a LH sampling, optimization methods are used to increase the space filling properties of the design. One of the most popular optimization algorithms for improvement of the LH sampling is the Max-Min optimization, which maximizes the minimum distance between any two sampling points. This creates a good coverage of the entire design space [22].

(a) Optimal Latin hypercube   (b) Bad Latin hypercube
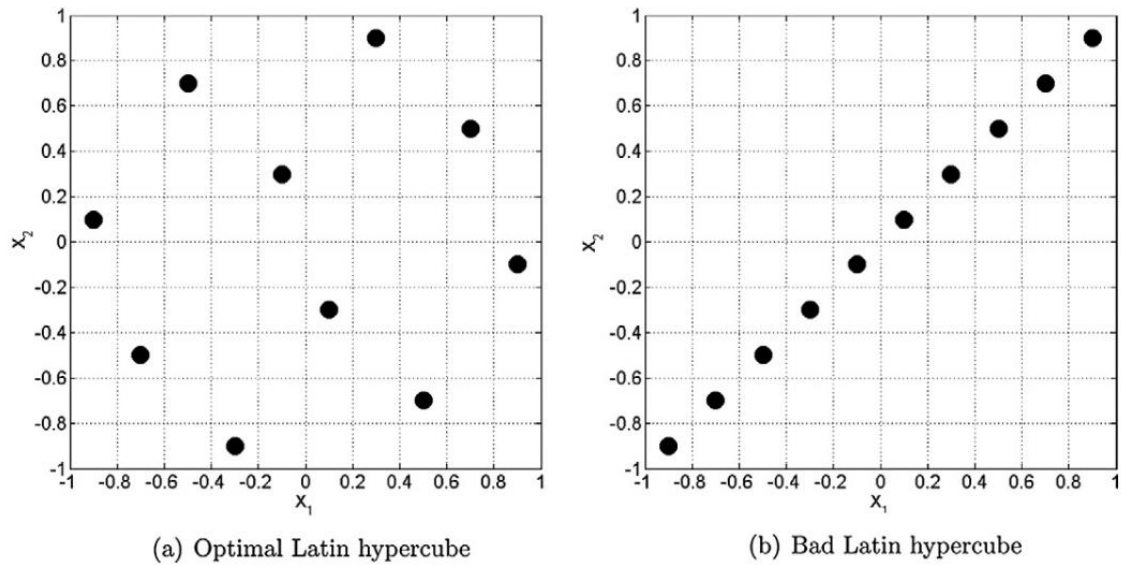
Figure 3.2: Schematic representation of LHC-sampling using max-min optimization (a) and possible sampling not using an optimization scheme (b) [22].

3.1.4 Conclusion Design of Experiments

For the Sensitivity Analysis of microstructure to Process Parameters it was decided that a Full Factorial Design would yield the best results. Because of the low number of process parameters (design variables) and levels, the number of simulations required for a full factorial design was feasible. Since the simulation was going to be validated using experimental data with discrete Process Parameters, the levels of the Full Factorial Design variables were also set to the experimental values. A table of the levels used for each Process Parameter can be found in **Table 3.1**.

The Latin Hypercube Design is also a feasible sampling strategy, but it would be difficult to compare its microstructure results with the experimental data because of the stochastic nature of LH. Also, the asymmetry of the given experimental process parameter set suggest using an Asymmetric Full Factorial Design over a symmetric Latin Hypercube Design approximation.

Table 3.1: List of Parameters used for the Full Factorial Design of the microstructure sensitivity analysis to Process Parameters

Laser Power [W]	Scan Speed [mm/s]	Layer Thickness [μm]
150,175,200	700,900,1100	0,20,30,40

3.2 Quantification of simulated Microstructure

The microstructure is a very complex that is difficult to analyze. Therefore, to make any viable claims on a given microstructure, a sub-set of quantities must be defined. These quantities create a common ground for the quantification and comparison of different microstructures. In this project three of these quantities were considered:

1. Grain Size / Aspect Ratio

2. Spatial Grain Orientation

3. Crystallographic Grain Orientation

The grain size can be defined differently based on the given data set. If the data set only consists of a two-dimensional slice, then the grain size is set to the average grain area of the set. If the data is a full three-dimensional set, then the grain size equates to the average grain volume. To define the average aspect ratio of the grains, methods like the linear intercept method [24,25] or the Principal Component Analysis can be used. Both methods will be explained in the following sub-chapters.

Spatial Grain Orientation is the quantification of the tilt angle of each grain. This quantity gives an intuitive understanding of how the grains are oriented in space. A main axis of each grain needs to be defined before the spatial grain orientation can be determined. This main axis is calculated to be the direction of highest variance, meaning longest direction of the grain. The method used for determination of Spatial Grain Orientation is the Principal Component Analysis.

Contrary to the Spatial Grain Orientation the Crystallographic Grain Orientation is not a quantity of the grain's geometry. It is a quantity that specifies the orientation of the crystal lattice inside the grain. This orientation is determined using the grain's Euler angles. To quantify the Crystallographic Grain Orientation Inverse Pole Figures and Texture Plots utilizing the MATLAB Toolbox MTEX were used. A detailed explanation of the quantification of Crystallographic Grain Orientation will be given in the following chapters.

3.2.1 Linear Intercept Method

The Linear Intercept Method is a technique based on the DIN EN ISO 643 [24] and the ASTM E 112 [25] norms. This technique is specialized in the quantification of grain size of two-dimensional data sets. It is very commonly used in quantification of experimental data. In the Linear Intercept Method, a grid of lines is projected onto a sample. Afterwards, each intersection between the lines and a grain boundary is marked. Each mark is assigned a value that represents the weight of that intersection. The weights are determined based on several rules [24,25]:

- When a line intersects a grain boundary it is weighted as 1

- Twin Grain Boundaries are not weighted

- When a line touches but doesn't intersect a grain boundary it is weighted as 0.5

- When a line intersects a triple point (Intersection point of three grains) it is weighted as 1.5

The true grain size $\bar{L}$ can then be calculated using the magnification M, the number of intersections $\sum x$ and the measured grain size L, which is given as the average distance between two intersection points [23]:

$$\bar{L} = \frac{\sum L}{M * \sum x}$$
(3.3)

There are two possible ways to apply the Linear Intercept Method. A depiction of the two methods can be found in **Figure 3.3.**
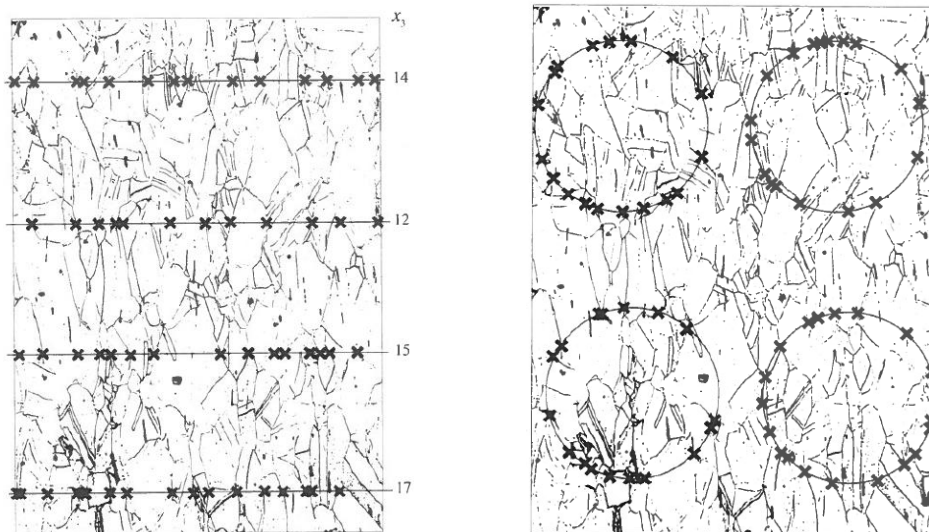

Figure 3.3: Representation of Linear Intercept method using straight lines (left) and circles (right) [23].

Since this method of characterizing grain size is only applicable to two-dimensional data and gives no information about the Spatial Grain Orientation it was not further considered in this project.

3.2.2 Principal Component Analysis (PCA)

The principal components of a collection of points in a real coordinate space are a sequence of p unit vectors, where the i-th vector is the direction of a line that best fits the data while being orthogonal to the first $i-1$ vectors [29]. With this an orthonormal basis is determined where different dimensions are linearly uncorrelated. This can be achieved by computing the eigenvalues and eigenvectors of the covariance matrix of a set of data points. The eigenvalues correspond to the variance in the direction of the corresponding eigenvector. The main axis of the set is then defined as the direction of the highest eigenvalue. [28]

To perform PCA on a general set of data points x , the set must first be standardized to have zero mean:

$$\bar{X} = x - \frac{\sum_{i=1}^{n} x_i}{n} \tag{3.4}$$

Preferably the values of the set should also be standardized to range from 0 to 1 in every dimension d. This is to ensure that dimensions of higher order have the same influence on the PCA.

$$X_d = \frac{\overline{X_d} - \min_i \overline{X_d}}{\max_i \overline{X_d} - \min_i \overline{X_d}} \qquad d \in 1, \dots, \#Dim \tag{3.5}$$

With this procedure the standardized set of data points X is generated. Afterwards, the estimation of the covariance matrix C is calculated as follows:

$$C = X^T X \tag{3.6}$$

Then the eigenvalues d_i of the covariance matrix are stored in a diagonal matrix D while the eigenvectors v_i are stored in a matrix V. The eigenvalues in matrix D are commonly ordered in an increasing sequence. A schematic representation of the Principal Component Analysis applied to multivariate Gaussian distribution can be found in **Figure 3.4**.
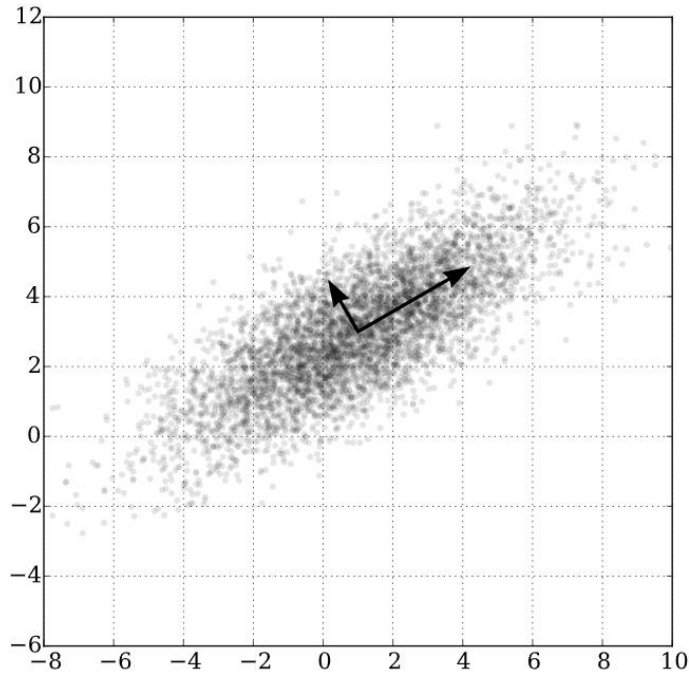
Figure 3.4: PCA applied to a multivariate Gaussian distribution
centered at (1,3). [29]

For the quantification of microstructure using PCA each grain is analyzed separately. The center positions of the cells, that make up a grain, are stored in the matrix x. Then PCA is applied to find the grain's main axis. Afterwards, all data points are projected onto the three principal directions and the maximum distance between any two points is calculated as:

$$\overline{p_i} = \frac{p_i \cdot v_k}{\|v_k\|} v_k \qquad\qquad (3.7)$$

$$d_k = \max\left(\|\overline{p_i} - \overline{p_j}\|\right) \quad k = 1,2,3 \qquad (3.8)$$

Where $\overline{p_i}$ is the projection of the data point p_i on the eigenvector v_k and d_k represents the maximum distance between either two projection points, which is used as a representative result for the grain's dimension in that direction.

With these three distances the grain shape can be quantified. The grain aspect ratio r is then determined as:

$$r = \frac{d_1}{\frac{(d_2 + d_3)}{2}} \qquad\qquad (3.9)$$

Where d_1 is the maximum distance between two points on the main axis and d_2 and d_3 are the maximum distance between two points on the off axes.

Using these results the Spatial Grain Orientation can be fully characterized.

3.2.3 Texture

The Principal Component Analysis gives a quantification of the geometrical properties of the microstructure. To fully quantify the microstructure a method for quantification of the Crystallographic Grain Orientation must be adapted. For a given microstructure its Texture is defined as the distribution of crystallographic orientations of a polycrystalline sample. If a sample has no or very weak texture it is said to have a random distribution. If there exists a preferred orientation, then a sample has a moderate or strong texture. Samples with strong textures tend to exhibit properties with a high level of anisotropy. A common technique for visualization of texture is the inverse pole figures. [32]

Because of the systematic temperature gradient directions during Selective Laser Melting, a moderate to strongly textured microstructure is expected. According to A. Leicht [31] the texture of a microstructure in SLM is dependent on the melt pool dimensions, see **Figure 3.5**.

There are two main approaches for the quantification of crystallographic orientation, namely its representation in a reference coordinate system using Euler angles or a representation of the crystallographic alignment with a physical direction (in this case the direction of highest temperature gradient). The latter is commonly used in research because of its independence on a macroscopic coordinate system, which makes it easier to compare microstructures from different sources. The main drawback of this method is its limitation to two-dimensional data sets. Since most experimental results are generated using sliced samples, this drawback is not an issue when comparing simulation results with experimental results. To mimic the two-dimensionality of experimental results the simulation data was virtually sliced, and the slices were analyzed using the MATLAB Toolbox MTEX. To this end the results of each slice were visualized in inverse pole figures.
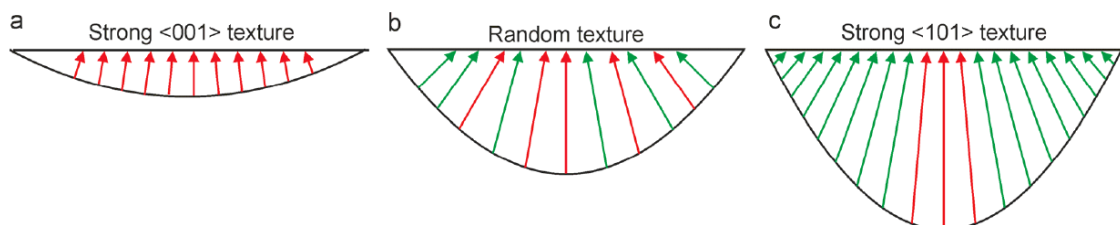

Figure 3.5: Schematic representation of the texture evolution with incrasing meltpool depth. [31]

4

Results and Discussion

In this chapter a summary of the results of the Microstructure Sensitivity Analysis to Process Parameters will be shown. First, a quick overview of the MATLAB tool used for data extraction will be given. Afterwards, the generated results will be displayed and discussed in detail.

4.1 Data Extraction

Early in this project it was decided that that for an efficient simulation of Selective Laser Melting Single Tracks, a tool must be developed that combines the thermal simulation from ABAQUS with the Cellular Automata Microstructure simulation in MATLAB. First the input parameters of the thermal simulation were defined to be:

- The Goldak heat source parameters (a, b, c_f, c_r)

- The absorptivity (α)

- The Process Parameters $(P_{laser}, v_{scan}, t_{layer})$

Where P_{laser} , v_{scan} , t_{layer} denote the laser power, laser scan speed and layer thickness, respectively. These predefined inputs should ensure a high enough flexibility for the design of experiments in future projects. After the design of each input has been chosen and saved in an excel file the tool then generates an appropriate input (.inp) file and starts the thermal simulation in ABAQUS.

For the simulation to be able to simulate the powder layer an ABAQUS subroutine was defined. This subroutine assigns a field variable, which represents the

current state of the node (powder or bulk), to the powder layer and the bulk material. During the simulation the subroutine checks in every time step which nodes in the powder layer have reached the melting temperature. If they reach the melting temperature their field variable is then be set to bulk. With this approach a powder layer could be simulated using continuum-based modelling. The different material properties used for bulk and powder can be found in **Table 4.1**.

Table 4.1: Table of material properties used in the thermal simulation

Material Properties		
Thermal Conductivity [$\frac{W}{mK}$]	Temperature [$°C$]	Field
9.1	25	Bulk
34	1260	Bulk
0.124	25	Powder
0.169	1260	Powder

After the thermal simulation has concluded the generated temperature data is then extracted from the dat-file (.dat) and stored in a MATLAB-File. Afterwards, the dat-file is deleted for memory reasons. The temperature data is then used for the determination of melt pool dimensions and for the simulation of microstructure. Finally, the melt pool data is stored, and the microstructure data is analyzed using the method explained in **Chapter 3.2**. The microstructure analysis was divided into two parts, namely the two-dimensional and three-dimensional analysis. This is to ensure that the generated microstructure can be validated using two-dimensional experimental data and can be analyzed in its full three-dimensional complexity. A schematic representation of the tool can be found in **Figure 4.1**.

Additionally, this tool was created in cooperation with Bardh Dervishaj, who was doing a sensitivity analysis of melt pool dimensions to process and modeling parameters. The tool was designed to be fully automated and easy to use. All the tool needs are an excel file with the predefined input parameter design.
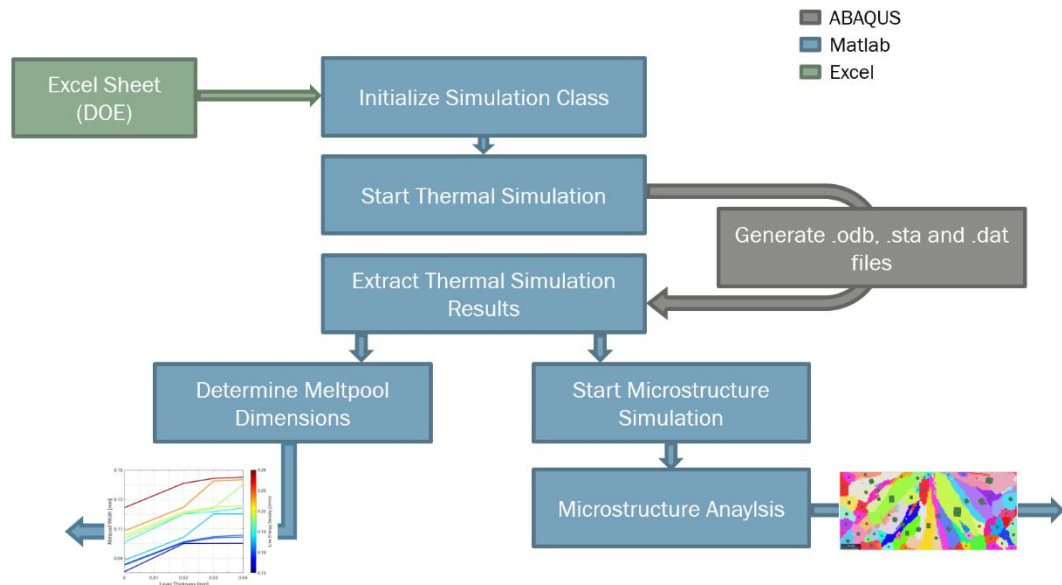
Figure 4.1: Schematic representation oft he MATLAB tool for microstructure and melt pool analysis.

4.2 Microstructure Sensitivity Analysis to Process Parameters

The Microstructure Sensitivity Analysis to Process Parameters was split into two main categories, namely the three-dimensional analysis and the two-dimensional analysis. The latter was then validated using experimental data.

4.2.1 Three-Dimensional Microstructure Analysis

To get a better understanding how the three-dimensional grain structure evolves during a Selective Laser Melting process, the grain's spatial orientation and geometries were first analyzed. For this, three main quantities were determined, namely the average grain aspect ratio, the grain's main axis angle α projected on the substrate plate and measured from the laser scan direction and the grain's main axis tilt angle β measured from the substrate plate towards the building direction. The quantities of each grain were then weighted based on its grain size, meaning that larger grains have a stronger influence on the data. This is to ensure a more intuitive understanding of what the average grain structure looks like without having to visualize the microstructure. These three quantities can give a very intuitive understanding of the spatial grain evolution.

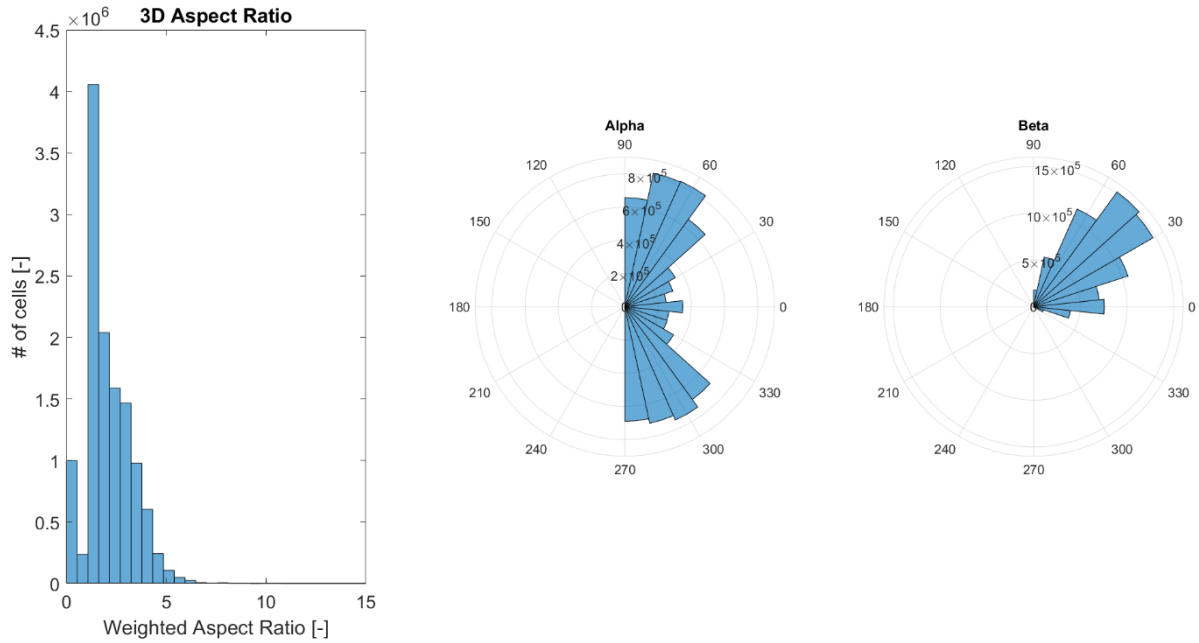A sample of this analysis can be found in **Figure 4.2**.

Figure 4.2: Sample result for the three-dimensional microstructure analysis with
$$P_{laser} = 200W \; v_{scan} = 700\left(\frac{mm}{s}\right) \; t_{layer} = 0 \; um.$$

As evident from **Figure 4.2** the microstructure shows to be very anisotropic since the grain's average aspect ratio is larger than 1.5. This aspect ratio hints at a columnar grain growth. Looking at the main axis angle α a clear trend of grains growing in a $\pm 60°$ direction seems to arise. This is not a surprising result, since grains lying outside of the laser path tend to grow towards the laser direction. This causes the grains further outside the laser path to have a higher magnitude of angle α. β on the other hand, shows a clear trend of columnar grain growth with a tilt angle of $40°$. This could also be explained by the tendency of columnar grains to grow in the direction of highest temperature gradient, which in this case is the direction towards the laser source. All in all, the three-dimensional microstructure shows to possess a columnar grain structure, in which most grains are growing towards the laser source in direction of highest temperature gradient. With this an intuitive understanding of the whole three-dimensional grain structure was achieved.

The final step in the analysis would be to look at the crystallographic grain structure, which is not possible with the current methods as discussed in **Chapter 3.2**. Therefore, the three-dimensional sensitivity analysis was continued without investigating the crystallographic properties.

To quantify the effects of Process Parameters to the microstructure evolution, the quantities were plotted against the Line Energy Density. The Line Energy Density E_{line} for a given set of Process Parameters is defined as:

$$E_{line} = \frac{P_{laser}}{v_{scan}} \qquad\qquad (4.1)$$

Where P_{laser} and v_{scan} are the laser power and laser scan speed, respectively. The results of this analysis can be found in **Figure 4.3.**
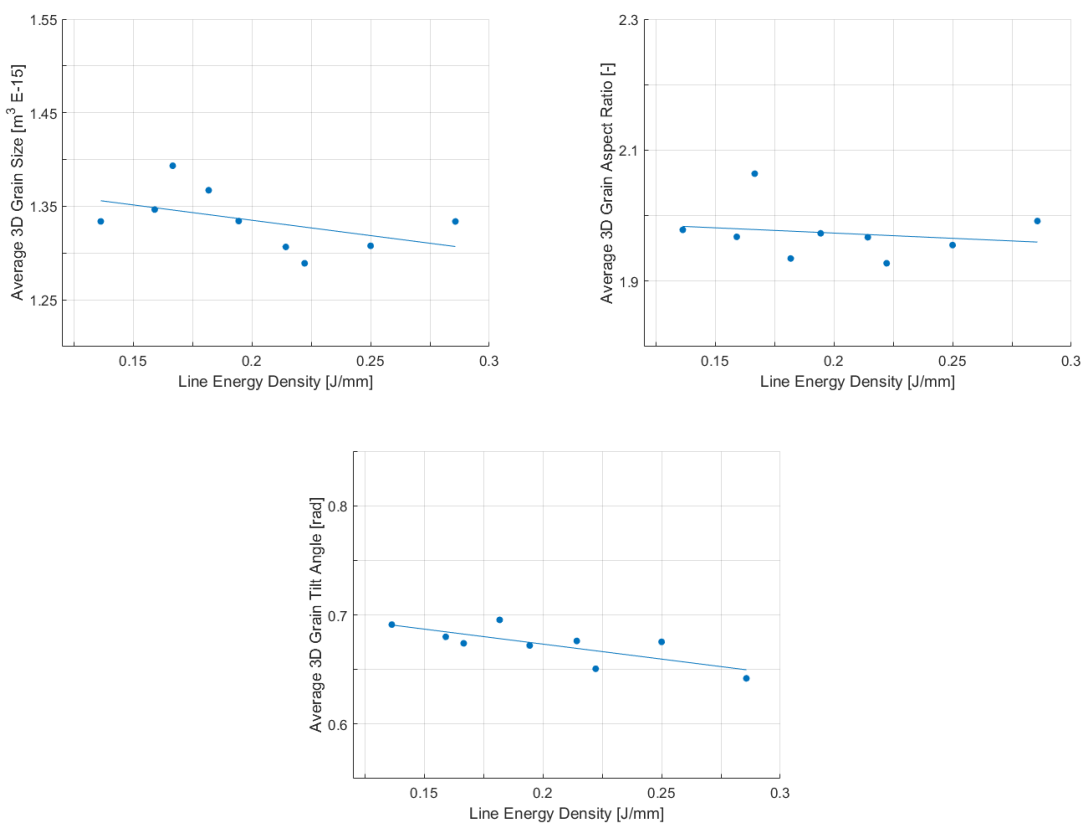

Figure 4.3: (top left) 3D grain size, (top right) 3D aspect ratio, (bottom) 3D tilt angle plotted against Line Energy Density

.

As evident from the above figure, the microstructure seems to produce finer grains with increasing Line Energy Density. An explanation for this can be the high temperature gradients with higher Line Energy Density and the therefore higher cooling rates. Interestingly, the average aspect ratio of microstructure seems to be mostly insensitive to the Line Energy Density with a slight tendency to decrease with increasing Line Energy Density. Lastly, the average tilt angle of the microstructure seems to decrease with increasing Line Energy Density. This can be attributed to the steeper temperature gradients at low Energy Densities.

To finalize the sensitivity analysis to Process Parameters the data was also plotted against the layer thickness, since the Line Energy Density does not account for changes in layer thickness. The results can be found in **Figure 4.4**.
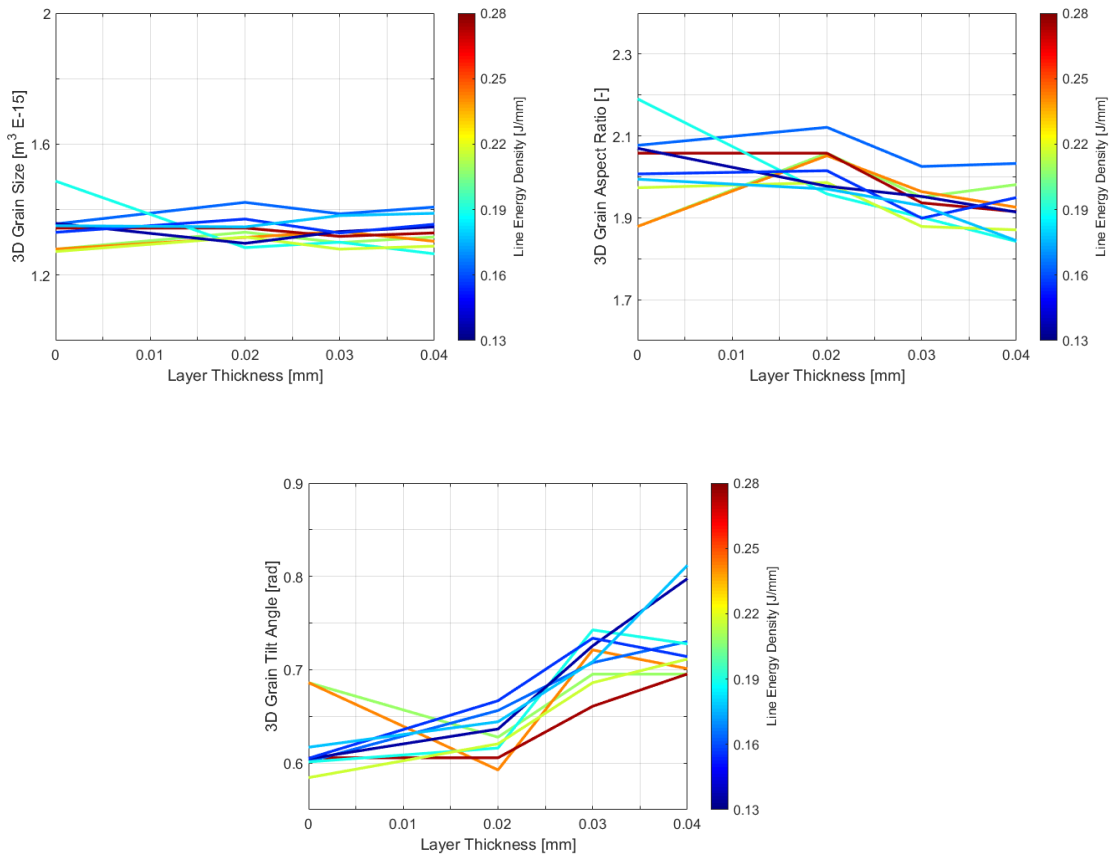

Figure 4.4: (top left) 3D grain size, (top right) 3D aspect ratio, (bottom) 3D tilt angle plotted against the layer thickness with a color ramp denoting the Line Energy Density

.
As seen from the figure the average grain size and aspect ratio seem to be insensitive to the layer thickness. This means that the grain geometries should not change with a change in layer thickness. The only changing quantity seems to be the tilt angle of the grains. Unusually, it increases with increasing layer thickness. This could be based on the low conductivity of the powder layer. This low conductivity could cause localization of heat in the powder layer and could steepen the tilt angle of the direction of highest temperature gradient. This would cause the grains to grow in a steeper direction and the grain geometries to stay the same. The steeper angle cannot be explained by a deeper melt pool since the melt pool depth is insensitive to Layer Thickness as shown by Bardh Dervishaj [40]. The figure also suggests different trends for different Line Energy Density levels, which could be explained by the fact that the vitalization uses linear interpolation functions and only one simulation was performed for each Design Point.

With this, the three-dimensional sensitivity analysis was concluded and the two-dimensional analysis with experimental data was continued.

4.2.2 Two-Dimensional Microstructure Analysis

The two-dimensional analysis was subdivided into two main categories, namely the analysis of grain shape (grain size / aspect ratio/ grain tilt angle) and the analysis of crystallographic grain orientation using inverse pole figures. These values were then compared with experimental results for an attempt of validating the simulation. Since at the time of this project only experimental results with a layer thickness of $t_{exp} = 0 \ \mu m$ were available the analysis was conducted with a constant layer thickness of $t_{sim} = 0 \ \mu m$.

First, the grain shape was analyzed by plotting the experimental data as well as the simulated data against the Line Energy Density. These results are depicted in **Figure 4.5.**
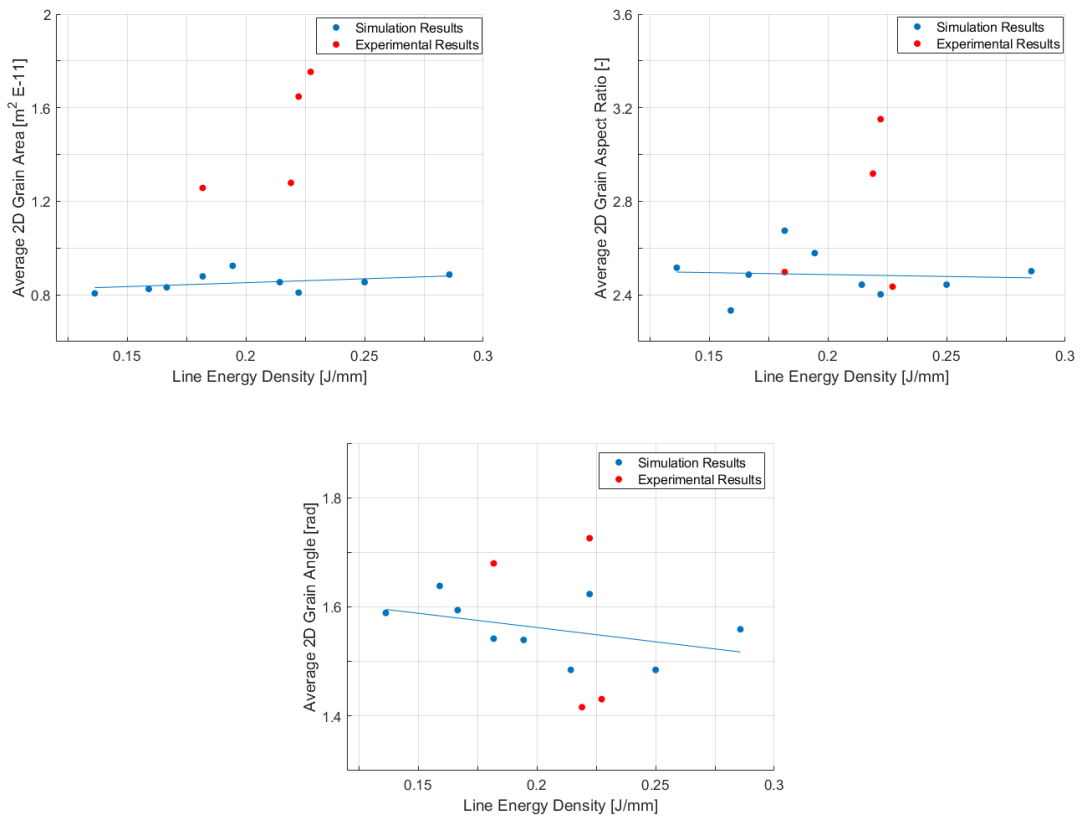

Figure 4.5: (top left) 2D grain size, (top right) 2D aspect ratio, (bottom) 2D tilt angle plotted against Line Energy Density, with simulation results in blue and experimental results in orange for a constant layer thickness $t_{layer} = 0 \ \mu m$

As seen in the first plot the simulation seems to always underpredict the grain size of the experimental results. A slight trend of increasing grain area with increasing Line Energy Density can also be observed for both data sets. The simulated data has a much smaller variance than the experimental one. This makes it difficult to compare the two results. The second plot shows that the simulated data suggests the two-dimensional aspect ratio to be insensitive to the Line Energy Density. Interestingly, the experimental data seems to coincide with

the simulating data for some of the values. But once again the experimental data has a much higher variance than the simulated data and hence makes it difficult to compare them. In the last plot a clear trend of decreasing tilt angle with increasing Line Energy Density was observed. Since this tilt angle is defined as the average angle between the transversal direction and the main axis direction measured towards the building direction, it has practically no real physical meaning. The experimental data seems to best fit this plot. But once again due to the high variance of the experimental data set it is hard to compare it to the simulated data set. All in all, the simulated data seems to consistently underpredict the average grain area and in general fit the average aspect ratio and tilt angle. But due to the high variance of the experimental data no conclusions could be drawn. More experimental data would be needed for a full validation of the simulation.

The Texture of the simulation and experimental data was analyzed using the MATLAB Toolbox MTEX. With this, the inverse pole figures were calculated and compared to the experimental data. A depiction of the results can be found in the following figures.

Figure 4.6: (top left) Orientation plot of experimental data (top right) Orientation Color Key (bottom) orientation plot of the simulated data. Orientation plots were indexed along the building direction. The Process Parameters for both plots are $P = 200W, v = 1100\frac{mm}{s}, t_{layer} = 0\mu m. E_{line} = 0.181818\frac{J}{mm}$
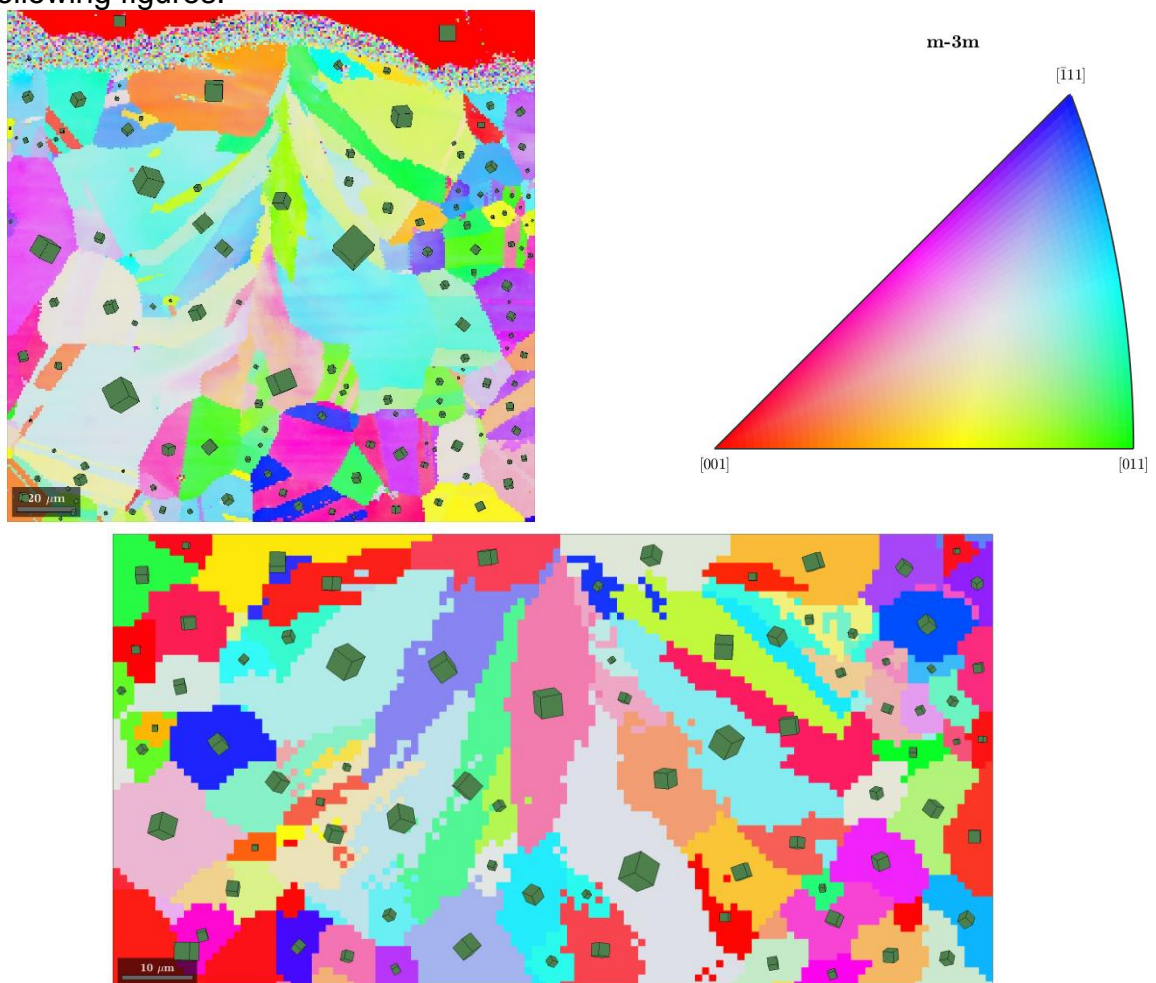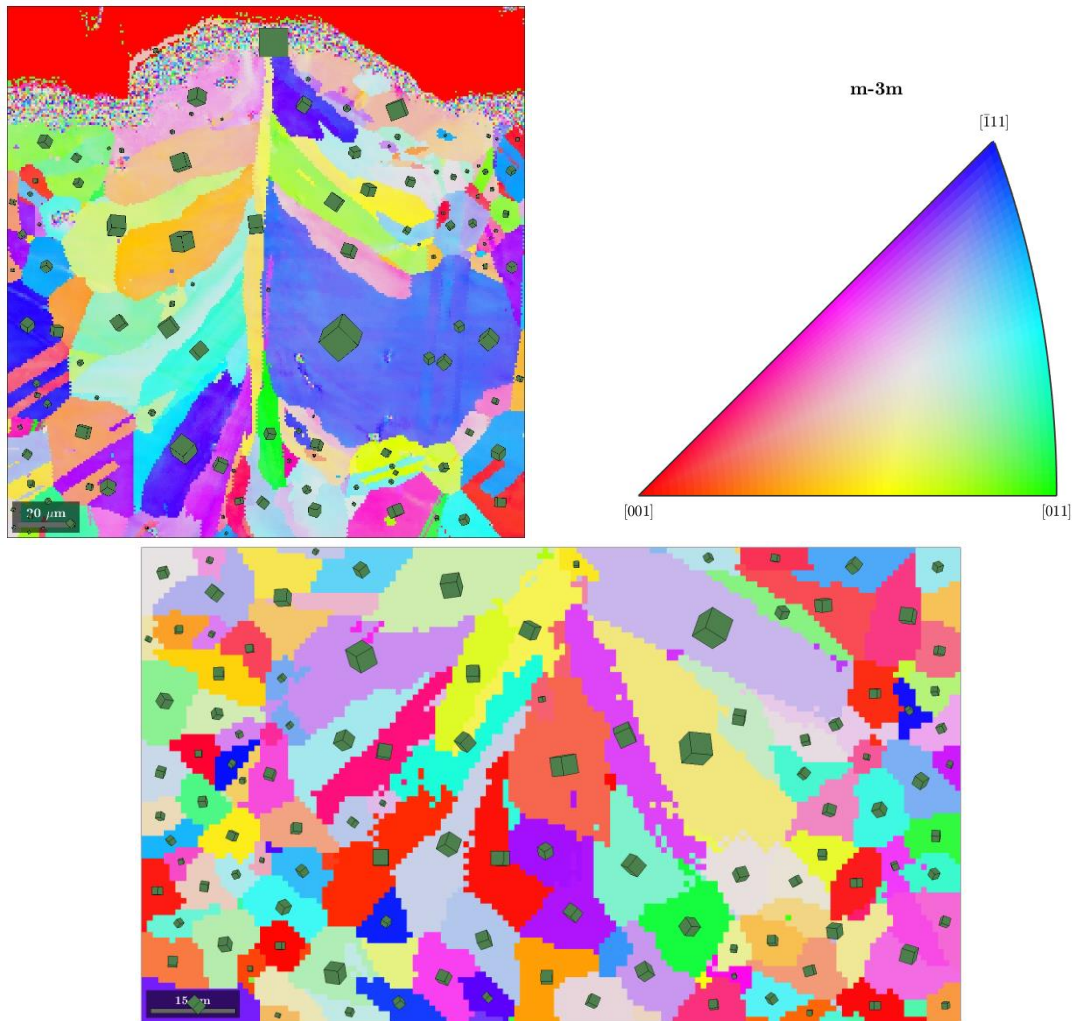
Figure 4.7: (top left) Orientation plot of experimental data (top right) Orientation Color Key (bottom) orientation plot of the simulated data. Orientation plots were indexed along the building direction. The Process Parameters for both plots are $P = 200W, v = 900\frac{mm}{s}, t_{layer} = 0\mu m.$ $E_{line} = 0.222222\frac{J}{mm}$

To compare these results quantitively the orientations were also plotted in an inverse pole figure. The results can be found in the following figures.
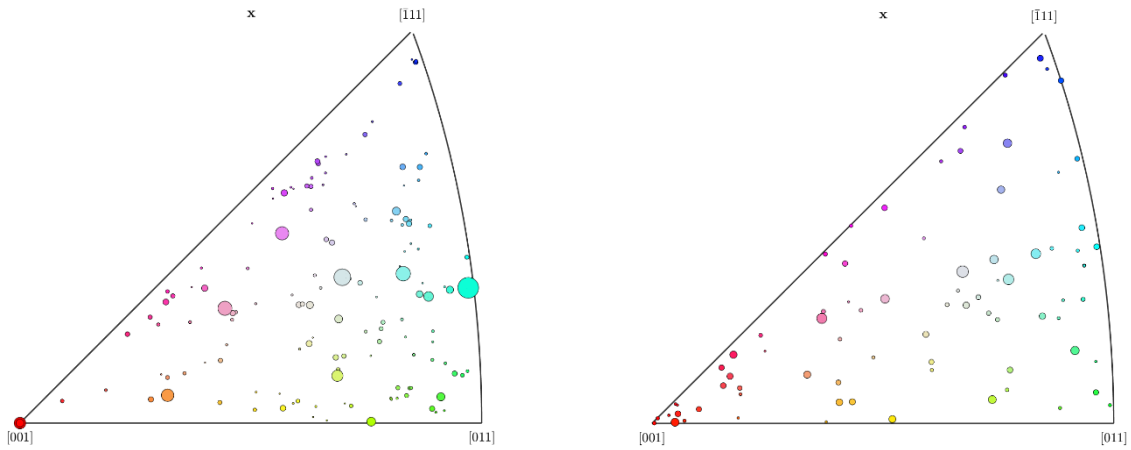

Figure 4.8: (left) Inverse Pole Figure of experimental Data, (right) Inverse Pole Figure of simulated data. Inverse pole plots were indexed along the building direction. The Process Parameters for both plots are $P = 200W, v = 1100 \frac{mm}{s}, t_{layer} = 0\mu m. E_{line} = 0.181818 \frac{J}{mm}$
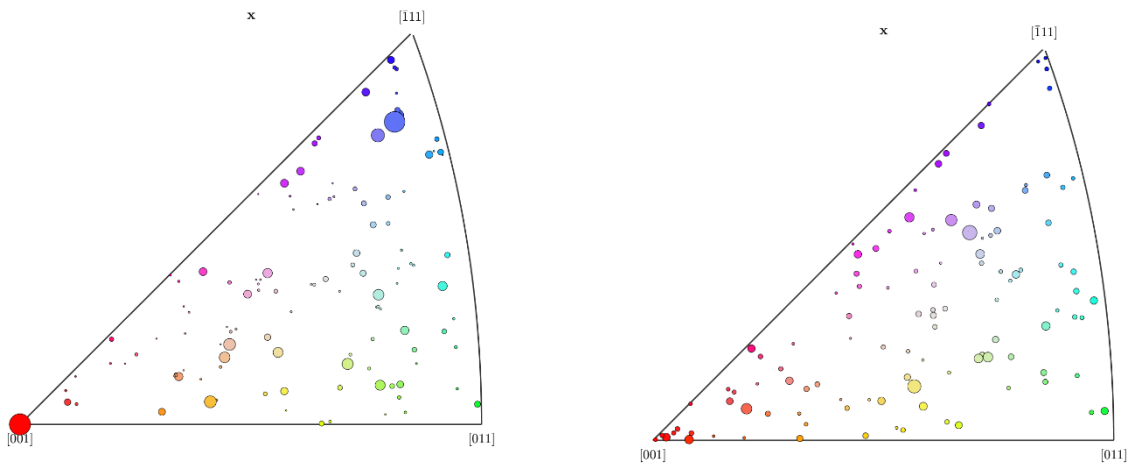

Figure 4.9: (left) Inverse Pole Figure of experimental Data, (right) Inverse Pole Figure of simulated data. Inverse pole plots were indexed along the building direction. The Process Parameters for both plots are $P = 200W, v = 900 \frac{mm}{s}, t_{layer} = 0\mu m. E_{line} = 0.222222 \frac{J}{mm}$

As evident from the figures above the experimental data seems to have a moderate [011] texture at low Line Energy Densities and a moderate [111] texture at higher Line Energy Densities. The simulation predicts a rather random texture at low Line Energy Densities whilst also predicting an increase in [111] texture at higher Line Energy Densities. Surprisingly, the simulation predicts a much stronger [001] texture in general. This is mostly likely due to the Update Rule used in the Cellular Automata simulation where the Decentered Octahedron Method tries to mimic the preferred growth directions of the unit cell. In the experiments this preferential growth direction is overshadowed by the fast cooling

rates and the short solidification times. Because this analysis was performed using a single-track simulation the presence of a strong texture evolution is not expected to develop. If the analysis was to be performed on a multi-layer simulation, then a strong texture of the columnar grains is expected to arise. In general, for the single-track simulation the resulting texture is arbitrary. Again, it was not possible to validate the simulation due to lack of experimental data.

34

5

Conclusion and Outlook

5.1 Conclusion

In this project an existing Selective Laser Melting Microstructure Simulation based on Cellular Automata was used to conduct a Sensitivity Analysis of Microstructure to Process Parameters. This analysis yielded the following conclusions:

- The MATLAB tool developed seems to be an efficient way to extract microstructure results whilst also incorporating Design of Experiment approaches

- Because of the strongly anisotropic and columnar grain growth during SLM conventional microstructure quantification methods like the Linear Intercept method are not appropriate

- The Principal Component Analysis provides a good approach for Grain Shape Quantification for three- and two-dimensional data sets

- Texture analysis can be used to quantify the Crystallographic Grain Orientation

- The average grain size and grain tilt angle decreases with increasing Line Energy Density, whilst the aspect ratio of the grains is insensitive to the Line Energy Density

- With increasing Layer Thickness, the tilt angle of the grains increases, whilst grain size and aspect ratio are insensitive to the Layer Thickness

- The two-dimensional analysis of simulation data compared to experimental data shows a much higher variance in the experimental data

- The simulations consistently underpredicts the grain area. The simulation predicts the aspect ratio and tilt angle well.

- Texture analysis shows a random texture for simulation data and experimental data for single tracks

- The simulation predicts a weak [001] texture for all Line Energy Densities while the experiments suggest a weak [011] texture for low Energy Densities and a weak [111] texture for high Energy Densities

- Due to lack of experimental data, it was not possible to validate the simulation

5.2 Outlook

For the continuation of this project the following topics should further be pursued:

- Generation of experimental data with varying Layer Thicknesses and Energy Densities

- Validation of the simulation with the new experimental data set

- Analysis of texture evolution parallel and perpendicular to scan direction

- Simulation of multi-layer Selective Laser Melting processes for a more general analysis of microstructure

- Generation of multi-layer experimental data for further validation of the simulations

Bibliography

[1]   Over, C., *Generative Fertigung von Bauteilen aus Werkzeugstahl X38CrMoV5-1 und Titan TiAl6V4 mit «Selective Laser Metling»,* Dissertation, Aachen (2003).

[2]   Doru Michael Stefanescu, Science and Engineering of Casting Solidification,

[3]   Maria L. Montero-Sistiaga et al., *Microstructure and mechanical properties of Hastelloy X produced by HP-SLM (high power selective laser melting),* 2019

[4]   Fude Wang, *Mechanical property study on rapid additive layer manufacture Hastelloy® X alloy by selective laser melting technology,* 2011

[5]   D. Tomus et al., *Influence of post heat treatments on anisotropy of mechanicalbehaviour and microstructure of Hastelloy-X parts produced byselective laser melting,* 2016

[6]   D. Tomus et al., *Controlling the microstructure of Hastelloy-X components manufactured by selective laser melting, 2013*

[7]   D. Tomus et al., *Effect of minor alloying elements on crack-formation characteristicsof Hastelloy-X manufactured by selective laser melting,* 2017

[8]   Y. Lian et al., *A parallelized three-dimensional cellular automaton model for grain growth during additive manufacturing,* 2018

[9]   J. A. Koepf et al., *3D multi-layer grain structure simulation of powder bed fusion additive manufacturing,* 2018

[10]   Ferreira AF, da Silva AJ, de Castro JA (2006) Simulation of the solidification of pure nickel via the phase-field method. Mater Res 9(4):349–356

[11]   I. Gholaminezhad et al., *Uncertainty quantification and robust modeling of selective laser melting process using stochastic multi-objective approach,* 2018

[12]   S. Hibino et al., *Control of Crystallographic Texture and Mechanical Properties of Hastelloy-X via Laser Powder Bed Fusion,* 2021

[13]   K.P. Hadler, J. Müller, *Cellular Automata: Analysis and Applications*, Springer, 2017

[14]   Mogg, O., *Simulation der Gefügeentwicklung bei Selective Laser Melting,* Bachelor thesis at Institut für Werkzeugmaschinen und Fertigung (IWF) at ETH Zürich, spring 2015

[15]   Lazaro Beltran-Sanchez, Doru M. Stefanescu, *Growth of Solutal Dendrites: A Cellular Automaton Model and Its Quantitative Capabilities,* 2002.

[16]   Amir Reza Ansari Dezfoli et al., *Determination and controlling of grain structure of metals after laser incidence: Theoretical approach*, 2017

[17]   Gandin C-A, Rappaz M (1997) A 3D cellular automaton algorithm for the prediction of dendritic grain growth. Acta Mater 45(5):2187–2195

[18]   Czitrom, V. (1999). One-Factor-at-a-Time versus Designed Experiments. *The American Statistician*, *53*(2), 126–131. https://doi.org/10.2307/2685731

[19]   Uhoraningoga A, Kinsella GK, Henehan GT, Ryan BJ. The Goldilocks Approach: A Review of Employing Design of Experiments in Prokaryotic Recombinant Protein Production. Bioengineering (Basel). 2018 Oct 19;5(4):89. doi: 10.3390/bioengineering5040089. PMID: 30347746; PMCID: PMC6316313.

[20]   J. A. Adepoju, R. A. Ipinyomi, *Construction of Asymmetric Fractional Factorial Designs*, 2016

[21]   Wu, C. F. Jeff et al., Experiments: Planning, analysis, and parameter design optimization, 2000

[22]   K. Cormbecq et al., *Efficient space-filling and non-collapsing sequential design strategies for simulation-based modeling*, 2011

[23]   Higgson, R.L., Sellars, C.M., *Worked Examples in Quantitative Metallography,* Maney, 2003.

[24]   DIN EN ISO 643, *Stahl – Mirkophotographische Bestimmung der erkennbaren Korngrösse,* 2017.

[25]   ASTM E112-10, *Standard Test Methods for Detemining Average Grain Size,* 2010.

[26]   http://www.metallograf.de/start.htm?/richtreihen/eniso643.htm, 2018

[27]   M. Yang et al., *Phase-field modeling of grain evolutions in additive manufacturing from nucleation, growth, to coarsening,* 2021

[28]   I. T. Jolliffe, *Principal Component Analysis*, 2002

[29]   https://en.wikipedia.org/wiki/Principal_component_analysis , 2021

[30]   Stander N., Roux W., Eggleston T., Craig K., LS-Opt User's Manual. LSTC, 2006

[31]   A. Leicht, *Laser powder bed fusion of 316L stainless steel Microstructure and mechanical properties as a function of process parameters, design and productivity*, Sweden 2020

[32]   https://en.wikipedia.org/wiki/Texture_(crystalline) , 2021

[33]   Badrossamay, M., Childs, T.H.C., *Further studies in selective laser melting of stainless and tool steel poweders,* International Journal of Machine Toold and Manufacture, 47, (2007), p. 779-784.

[34]   Yasa, E., Kurth, J.-P., *Microstructural inverstigation of Selective Laser Melting 316L stainless steel parts exposed to laser remelting,* Proceeding Engineering, 91, (2011), p. 389-395.

[35]   R.Song, et al., *Grain boundary characterization and grain size measurement in an ultrafine-grained steel*, 2004

[36]   Eckard M., Hans-Werner Z., *Praktikum in Werkstoffkunde* ,11.Auflage, 2011

[37]   W.J. Böttinger, et al., *Modeling of Casting, Welding and Advanced Solidification Process-VI*, TMS Publications, 1993

[38]   D. Wang, et al., *Investigation of crystal growth mechanism during selective laser meltingand mechanical property characterization of 316L stainless steel parts*, 2016

[39]   Thorsten Heeling, et. al., *Melt pool simulation for the evaluation of process parameters inselective laser melting,* 2017

[40]   Ba. Dervishaj, *Sensitivity Analysis of Meltpool Dimensions and Optimization of modeling Parameters using SLM thermal Single Track Simulations of Hastelloy X*, 2021